

Effects of strain on the flat band in twisted bilayer graphene

Zhen Zhang(张镇), Lu Wen(文露), Youkai Qiao(乔友凯), and Zhiqiang Li(李志强)
Citation: Chin. Phys. B, 2023, 32 (**10**): 107302. DOI: 10.1088/1674-1056/acb2c1

Journal homepage: http://cpb.iphy.ac.cn; http://iopscience.iop.org/cpb

What follows is a list of articles you may be interested in

Epitaxial growth of trilayer graphene moiré superlattice

Yalong Yuan(袁亚龙), Yanbang Chu(褚衍邦), Cheng Hu(胡成), Jinpeng Tian(田金朋), Le Liu(刘乐), Fanfan Wu(吴帆帆), Yiru Ji(季怡汝), Jiaojiao Zhao(赵交交), Zhiheng Huang(黄智恒), Xiaozhou Zan(昝晓洲), Luojun Du(杜罗军), Kenji Watanabe, Takashi Taniguchi, Dongxia Shi(时东霞), Zhiwen Shi(史志文), Wei Yang(杨威), and Guangyu Zhang(张广宇)
Chin. Phys. B, 2023, 32 (**7**): 077304. DOI: 10.1088/1674-1056/accdc8

Periodic electron oscillation in coupled two-dimensional lattices

Yan-Yan Lu(陆艳艳), Chao Wang(王超), Jin-Yi Jiang(将金益), Jie Liu(刘洁), and Jian-Xin Zhong(钟建新)
Chin. Phys. B, 2023, 32 (**7**): 070306. DOI: 10.1088/1674-1056/acce93

Gate-controlled localization to delocalization transition of flat band wavefunction in twisted monolayer-bilayer graphene

Siyu Li(李思宇), Zhengwen Wang(王政文), Yucheng Xue(薛禹承), Lu Cao(曹路), Kenji Watanabe, Takashi Taniguchi, Hongjun Gao(高鸿钧), and Jinhai Mao(毛金海)
Chin. Phys. B, 2023, 32 (**6**): 067304. DOI: 10.1088/1674-1056/acc805

Machine learning of the Γ-point gap and flat bands of twisted bilayer graphene at arbitrary angles

Xiaoyi Ma(马宵怡), Yufeng Luo(罗宇峰), Mengke Li(李梦可), Wenyan Jiao(焦文艳), Hongmei Yuan(袁红梅), Huijun Liu(刘惠军), and Ying Fang(方颖)
Chin. Phys. B, 2023, 32 (**5**): 057306. DOI: 10.1088/1674-1056/acb2c3

Spin- and valley-polarized Goos-Hänchen-like shift in ferromagnetic mass graphene junction with circularly polarized light

Mei-Rong Liu(刘美荣), Zheng-Fang Liu(刘正方), Ruo-Long Zhang(张若龙), Xian-Bo Xiao(肖贤波), and Qing-Ping Wu(伍清萍)
Chin. Phys. B, 2023, 32 (**3**): 037301. DOI: 10.1088/1674-1056/ac89e2

Effects of strain on the flat band in twisted bilayer graphene

Zhen Zhang(张镇), Lu Wen(文露), Youkai Qiao(乔友凯), and Zhiqiang Li(李志强)†

College of Physics, Sichuan University, Chengdu 610064, *China*

(Received 16 September 2022; revised manuscript received 10 January 2023; accepted manuscript online 13 January 2023)

Based on the effective continuum model, we systematically study the electronic band structures and density of states of twisted bilayer graphene near the magic angle under the influence of different types of strain, including shear strain, volume-preserving strain and biaxial strain. We find that the flat bands behave very differently under various types of strain. Volume-preserving strain generically leads to broader van Hove singularities associated with the flat bands compared with those under shear strain, with dissimilar strain direction dependence. The band structures and density of states under shear and volume-preserving strains change with the strain direction, while those under biaxial strain are independent of the direction of strain. In particular, the effect of biaxial strain on twisted bilayer graphene is geometrically and electronically similar to the influence of the twisted angle. Our results reveal the characteristic structures in the band structures and density of states under various types of strain, which can serve as fingerprints for exploring the effects of strain on the novel physics of this system.

Keywords: graphene, moiré superlattice, magic angle and strain

PACS: 73.22.Pr, 73.21.Cd, 81.05.ue **DOI:** 10.1088/1674-1056/acb2c1

1. Introduction

Many correlated and topological electronic phases have been discovered in twisted bilayer graphene (TBG) in recent studies,[1–19] which has led to an outburst of research based on this system over the past few years.[20–23] These novel quantum states originate from the formation of flat electronic bands near a magic twisted angle ($\sim 1^\circ$) under the influence of the moiré superlattice.[20–37] Such flat bands exhibit a sensitive dependence on small lattice deformations[24,38] that are induced by lattice relaxation or strain. On the other hand, strain is an effective tool for engineering the flat bands[24,39] and thus helps us understand the various exotic quantum states in TBG.

Previous experimental[8] and theoretical works[24,36,39–41] have shown that applying a heterostrain (relative strains between layers) in a two-layer structure can significantly modify the band structures and electronic phases. Due to the interaction between substrate and graphene in the preparation process, various strains are prevalent in actual TBG samples. Therefore, it is of great significance to study the effect of different types of strain on the flat bands in TBG. The influence of uniaxial heterostrain on the bands of TBG has been explored in detail in previous studies.[24,38,42,43] However, there are few detailed studies[39,44] on the difference and connection between the effects of various types of strains on the electronic structure of TBG.

In this paper, we systematically investigate the effect of different heterostrains on the moiré band structures and density of states (DOS) of TBG based on a low-energy effective continuum model. We show that various strains strongly affect the band structures of TBG near the magic angle. Compared with the twisted angle, only a small magnitude of strain is required to cause separation between the conduction band and the valence band. Volume-preserving strain can broaden the van Hove singularities compared with shear strain, and both types of strain have dissimilar dependence on strain direction. In addition, unlike other strains, the effect of biaxial strain on TBG is very similar to that of the twisted angle both geometrically and electronically. Therefore, certain angles that are difficult to achieve during sample fabrication experimentally can be replaced by applying biaxial strain. The effects of dissimilar strains on the band structures and DOS have very subtle differences, which can be used to experimentally distinguish various types of strain. Our findings regarding the flat bands and van Hove singularities have broad implications for the novel quantum phases in TBG, which can be directly studied by scanning tunnelling microscopy (STM) experiments.[6–8,17]

2. Theoretical background

For TBG without strain, where the two graphene layers are only rotated relative to each other, the moiré superlattice forms an array of equilateral triangular domains with alternating AB and BA stacking regions. However, the moiré pattern and the corresponding Brillouin zone of TBG are significantly distorted in the presence of heterostrain. An example of the associated moiré pattern generated with various strains is shown in Fig. 1. Because the moiré superlattice period is much larger than the atomic scale in the limit of the small twisted angle, the continuum model can efficiently capture low-energy electronic structures,[20,29,45] which allows us to analyze the effect of geometrical deformation (including the twisted angle and strain) on the physical properties of TBG.

†Corresponding author. E-mail: zhiqiangli@scu.edu.cn

© 2023 Chinese Physical Society and IOP Publishing Ltd

In this section, we first elaborate on the effect of deformation on the properties of monolayer graphene. The primitive vectors of single-layer graphene are $\boldsymbol{A}_1 = a(1,0)$ and $\boldsymbol{A}_2 = a(1/2, \sqrt{3}/2)$, where $a \approx 0.246$ nm is the lattice constant of graphene. Thus, the reciprocal vectors are defined as $\boldsymbol{G}_1 = \frac{2\pi}{a}(1, -1/\sqrt{3})$ and $\boldsymbol{G}_2 = \frac{2\pi}{a}(0, 2/\sqrt{3})$. Then, we consider applying a variety of geometrical deformations $\mathcal{E}$ to single-layer graphene. In the case of the small deformation limit, $\mathcal{E}$ can be represented by a matrix[24]

$$\mathcal{E} = \begin{pmatrix} \epsilon_{xx} & \epsilon_{xy} - \theta \\ \epsilon_{xy} + \theta & \epsilon_{yy} \end{pmatrix} = S(\epsilon) + T(\theta). \tag{1}$$

Here the antisymmetric part, labeled by $T(\theta)$, represents a rotation matrix with twisted angle θ. The symmetric part, labeled by $S(\epsilon)$, represents the strain with magnitude ϵ. Obviously, the shape of the unit cell as well as the Brillouin zone are both geometrically affected by deformation $\mathcal{E}$. Therefore, the rescaled primitive and reciprocal lattice vectors can be expressed as[24]

$$\boldsymbol{A}_i' = (\mathrm{II} + \mathcal{E})\,\boldsymbol{A}_i, \quad \boldsymbol{G}_i' = \left(\mathrm{II} - \mathcal{E}^{\mathrm{T}}\right)\boldsymbol{G}_i. \tag{2}$$

Here $\boldsymbol{A}_i$ and $\boldsymbol{G}_i$ $(i = 1, 2)$ refer to the primitive vectors and the reciprocal vectors without deformation, respectively.

For a TBG system, a periodic variation of the layer stacking order can emerge with a small value of deformation $\mathcal{E}$, as shown in Fig. 1. In our calculation, we consider a TBG system starting with AA stacking and then apply various geometrical deformations $\mathcal{E}$. Hence, the reciprocal lattice vectors $\boldsymbol{g}_i$ and the primitive lattice vectors $\boldsymbol{a}_i$ of the moiré superlattice[24] are

$$\boldsymbol{g}_i = \mathcal{E}^{\mathrm{T}}\boldsymbol{G}_i, \quad \boldsymbol{a}_i = \mathcal{E}^{-1}\boldsymbol{A}_i, \tag{3}$$

respectively. Here, $\mathcal{E} = \mathcal{E}_2 - \mathcal{E}_1$ is the relative deformation matrix between two layers of graphene, where $\mathcal{E}_l$ $(l = 1, 2)$ represents the deformation acting on each single layer of graphene. In this paper, the respective deformation of each layer is regarded as $\mathcal{E}_1 = -\mathcal{E}_2 = \mathcal{E}/2$, that is, the two graphene layers are rotated and strained oppositely with the same magnitude.

Based on the effective continuum model, the Hamiltonian of TBG can be written as

$$H = \begin{pmatrix} h_1 & U^{\dagger} \\ U & h_2 \end{pmatrix}, \tag{4}$$

where U is the interlayer coupling of two graphene layers and h_l $(l = 1, 2)$ is the intralayer Hamiltonian of layer l, which is given by the two-dimensional gapless Dirac equation[24]

$$h_l(\boldsymbol{k}) = \sum_{\xi=\pm} -\hbar v_{\mathrm{F}}/a \left[\left(\mathrm{II} + \mathcal{E}_l^{\mathrm{T}}\right)\left(\boldsymbol{k} - \boldsymbol{D}_{l,\xi}\right)\right] \cdot (\xi\sigma^x, \sigma^y). \tag{5}$$

In Eq. (5), $\xi = \pm$ labels the K (K') valley and σ^x (σ^y) is the Pauli matrix in the sublattice space. In the following calculations, we take $\hbar v_{\mathrm{F}}/a \approx 2.1354$ eV.[25] Within a simple two-center approximation and the small-strain limit, the position of the Dirac fermion $\boldsymbol{D}_{l,\xi}$ in momentum space is[24]

$$\boldsymbol{D}_{l,\xi} = \left(\mathrm{II} - \mathcal{E}_l^{\mathrm{T}}\right)\boldsymbol{K}_{l,\xi} - \xi\boldsymbol{A}, \tag{6}$$

with

$$\boldsymbol{A} = \frac{\sqrt{3}}{2a}\beta\left(\epsilon_{xx} - \epsilon_{yy}, -2\epsilon_{xy}\right), \tag{7}$$

where $\boldsymbol{K}_{l,\xi}$ denotes the location of the K (K') valley for layer l and $\boldsymbol{A}$ is the strain-induced vector potential.[24,46] In the $\boldsymbol{A}$ term, the hopping modulus factor is $\beta \approx 3.14$[46] and ϵ_{xx} (ϵ_{yy}, ϵ_{xy}) represents the component of the two-dimensional strain tensor.

Moreover, the effective interlayer coupling U is given by[20,24]

$$\begin{aligned} U = &\begin{pmatrix} u & u' \\ u' & u \end{pmatrix} + \begin{pmatrix} u & u'\omega^{-\xi} \\ u'\omega^{\xi} & u \end{pmatrix} \mathrm{e}^{\mathrm{i}\xi\boldsymbol{g}_1\cdot\boldsymbol{r}} \\ &+ \begin{pmatrix} u & u'\omega^{\xi} \\ u'\omega^{-\xi} & u \end{pmatrix} \mathrm{e}^{\mathrm{i}\xi(\boldsymbol{g}_1+\boldsymbol{g}_2)\cdot\boldsymbol{r}}, \end{aligned} \tag{8}$$

where $\omega = \mathrm{e}^{2\pi\mathrm{i}/3}$ and u and u' are the amplitudes of the diagonal and off-diagonal terms in the sublattice space, respectively.[47] They reflect the influence of lattice ripples on the moiré band structures. In particular, in the small-deformation regime, competition between the interlayer interaction and the elastic energy at the interface can lead to significant lattice relaxation for TBG. The reconstruction can be taken into account by using $u = 0.0797$ eV and $u' = 0.0975$ eV in our calculation, which are the interlayer coupling strengths of AA/BB and AB/BA stacked regions, respectively.[33,47]

In the following, we introduce into the effective Hamiltonian four different types of strain that are common in two-dimensional materials, namely, shear strain S_{sh}, volume-preserving strain S_{vp}, biaxial strain S_{ba} and uniaxial strain S_{ua}. In Fig. 1, we display the corresponding moiré pattern and the moiré Brillouin zone under various strains with magnitude $\epsilon = 0.7\%$ for TBG near the magic angle ($\theta = 1.05^{\circ}$). Four general forms of strain have been derived in detail in previous reports.[24,44] In addition, to further understand the effect of strain direction on the electronic band structures of TBG, we consider an angle φ of strain relative to the A1 axis (four-axis coordinate system) in our system.[8] Therefore, the strain tensor can be modified to the following form:[24,44]

$$S_{\mathrm{sh}} = R(\varphi)^{-1}\begin{pmatrix} 0 & \epsilon \\ \epsilon & 0 \end{pmatrix} R(\varphi) = \epsilon\begin{pmatrix} 2\cos(\varphi)\sin(\varphi) & \cos(\varphi)^2 - \sin(\varphi)^2 \\ \cos(\varphi)^2 - \sin(\varphi)^2 & -2\cos(\varphi)\sin(\varphi) \end{pmatrix}, \tag{9}$$

$$S_{\mathrm{vp}} = \epsilon\begin{pmatrix} \cos(\varphi) & \sin(\varphi) \\ \sin(\varphi) & -\cos(\varphi) \end{pmatrix}, \tag{10}$$

$$S_{\rm ba} = R(\varphi)^{-1}\begin{pmatrix}\epsilon & 0\\ 0 & \epsilon\end{pmatrix}R(\varphi) = \epsilon\begin{pmatrix}\cos(\varphi)^2+\sin(\varphi)^2 & -\cos(\varphi)\sin(\varphi)+\cos(\varphi)\sin(\varphi)\\ \cos(\varphi)\sin(\varphi)-\cos(\varphi)\sin(\varphi) & \sin(\varphi)^2+\cos(\varphi)^2\end{pmatrix} = \epsilon\begin{pmatrix}1 & 0\\ 0 & 1\end{pmatrix}, \quad (11)$$

$$S_{\rm ua} = R(\varphi)^{-1}\begin{pmatrix}-\epsilon & 0\\ 0 & \nu\epsilon\end{pmatrix}R(\varphi) = \epsilon\begin{pmatrix}-\cos(\varphi)^2+\nu\sin(\varphi)^2 & (1+\nu)\cos(\varphi)\sin(\varphi)\\ (1+\nu)\cos(\varphi)\sin(\varphi) & -\sin(\varphi)^2+\nu\cos(\varphi)^2\end{pmatrix}. \quad (12)$$

The above four strains are characterized by the strain magnitude ϵ and the direction φ. Here, the parameter $\nu = 0.16$ is the Poisson ratio[8] for graphene. Then, the deformation matrix $\mathcal{E}$ containing the strain direction φ and magnitude ϵ is obtained for TBG, and is of the form $\mathcal{E} = S(\epsilon\varphi)+T(\theta)$.

3. Results and discussion

Based on the effective continuum model described above, we calculate the electronic band structures of TBG at a fixed twisted angle $\theta = 1.05^\circ$ close to the magic angle under four different types of strain. In this article, the path of band structures is along the line $k_1 \to \gamma \to k_2 \to M \to \gamma \to M \to k_1$ in the moiré Brillouin zone scheme, as shown by the red dashed line in Fig. 1(a). In addition, we also perform a series of controls on the electronic band structures by varying the strain magnitude ϵ and direction φ. These results are fully displayed and discussed in this section.

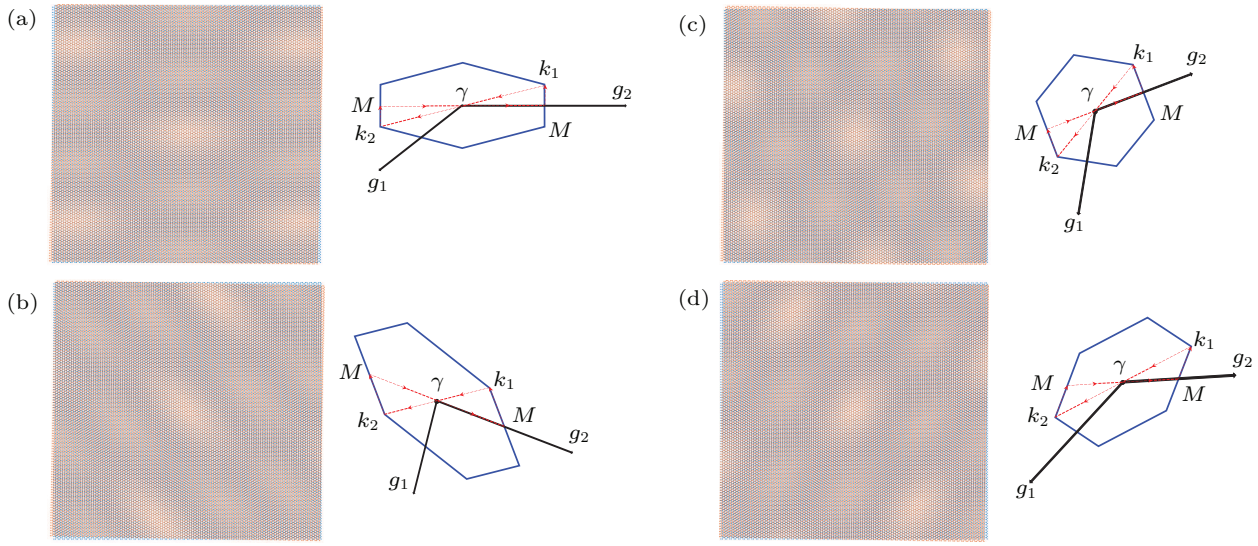


Fig. 1. Schematic representation of the moiré pattern and moiré Brillouin zone for TBG with a twisted angle $\theta = 1.05^\circ$ under the influence of four types of uniform strain along the armchair direction, namely, (a) shear strain, (b) volume-preserving strain, (c) biaxial strain and (d) uniaxial strain. The parameters of these strains are magnitude $\epsilon = 0.7\%$ and direction $\varphi = 0^\circ$. The red dashed line in (a) represents the momentum path for the energy band plots.

3.1. Shear strain

Interlayer and interfacial shear strain play crucial roles in the performance and application of TBG. However, the key parameters controlling shear strain have been poorly studied both experimentally and theoretically. Note that the form of shear strain considered in Eq. (9) is similar to that in the research of Koshino *et al.*,[39] and our form is equivalent to that in Ref. [39] under certain conditions. In particular, the shear strain form we considered is of more universal and practical significance, and can be combined with experimental studies.[48–51]

In Fig. 2, we show the band structures and DOS of the TBG system under shear strain with various magnitudes ϵ and directions φ. When the strain magnitude $\epsilon = 0$, TBG exhibits flat bands with vanishing band velocity near the charge neutral point (CNP), resulting from competition between the kinetic energy and the interlayer hybridization energy. Correspondingly, as shown by the black line in Figs. 2(a) and 2(b), the DOS has a strong peak near the CNP. However, the flat bands near the CNP are very sensitive to variation of the strain magnitude ϵ, and even a small magnitude of $\epsilon = 0.1\%$ causes them to split significantly, as shown in Figs. 2(a) and 2(b). Moreover, as the magnitude ϵ of strain increases, the energy separation of the lowest conduction band and valence band increases systematically. Then, the corresponding peaks in the DOS also shift systematically to higher energies with increase in ϵ. Unlike flat band features, the remote bands are slightly affected by the strain magnitude ϵ. Although the energy gap between the flat bands and the higher-energy bands becomes smaller with increase in ϵ, the two are not connected and still maintain a small energy gap of $\Delta \sim 0.24$ meV. Moreover, the energy shift of the two flat bands mainly occurs at the γ point, and the band dispersion is also mainly distributed near the γ point. The two bands are quite flat in most other regions of the Brillouin zone. In particular, shear strain does not open the gap

near the CNP due to the symmetry of $C_{2z}T$, and the conduction band and valence band are still connected by a Dirac crossing point. Because the threefold rotational symmetries are broken by the strain, the two Dirac crossing points are no longer located at the corners of the Brillouin zone but at a generic point.[24,38]

Compared with the strain magnitude ϵ, the electronic band structures of TBG are almost insensitive to the strain direction φ, as shown in Fig. 2(c). This is because the behavior of the flat band is highly correlated with the asymmetric and anisotropic components of the strain tensor.[39] However, the structure of van Hove singularities changes subtly with various strain directions φ. It can be clearly observed from Figs. 2(a) and 2(b) that the DOS shows one or two smooth main peaks at $\varphi = 30°$ and 9°, while the prominent peaks of the DOS exhibit some shoulders and the van Hove singularities are broadened when the direction φ deviates by 30° or 90°. In addition, the system is periodic for $\varphi \to \varphi + \pi/3$ originating from the symmetry of the unstrained system. Thus, the DOS of TBG with shear strain also goes through periodic changes.

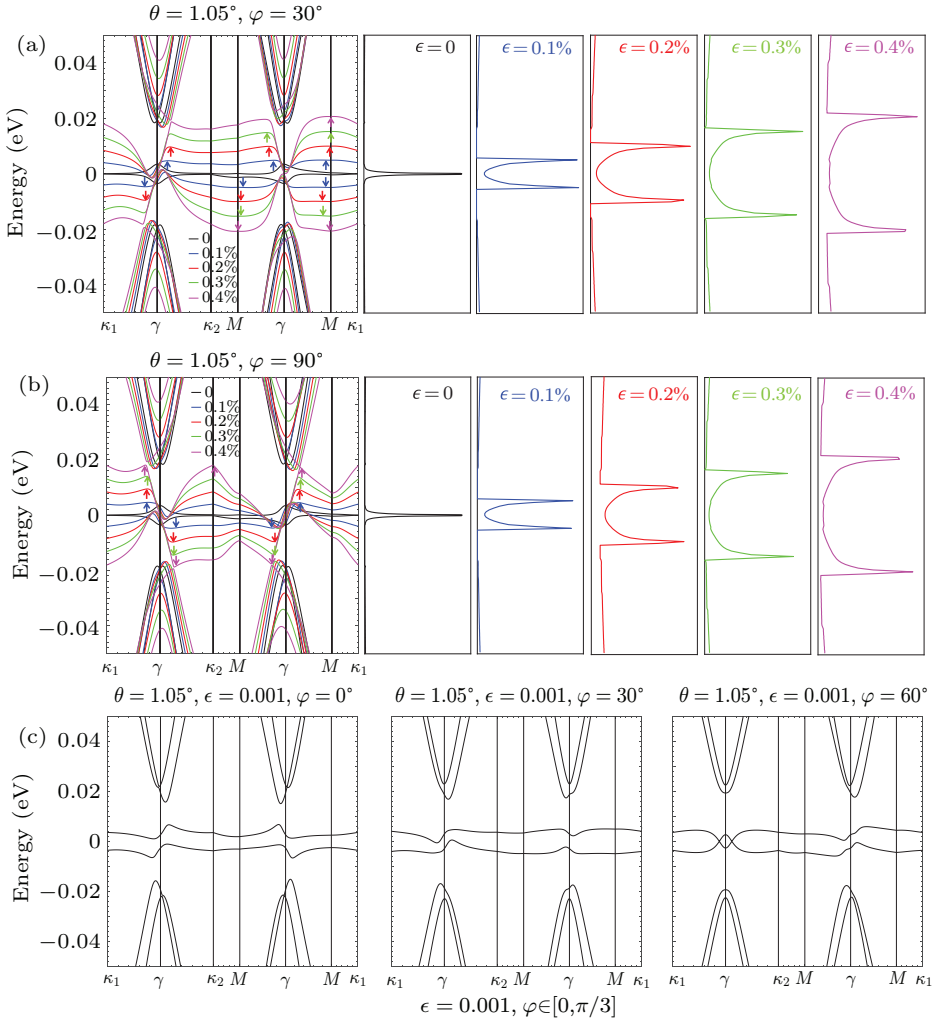


Fig. 2. Band structures and the DOS of magic angle TBG considering the shear strain. (a) Strain direction $\varphi = 30°$ and magnitude $\epsilon = 0, 0.1\%, 0.2\%, 0.3\%, 0.4\%$. (b) Strain direction $\varphi = 90°$ and magnitude $\epsilon = 0, 0.1\%, 0.2\%, 0.3\%, 0.4\%$. Different colors represent different magnitudes of strain. The colored arrows mark the energy corresponding to the van Hove singularities. (c) The band structures of different directions φ with the strain magnitude $\epsilon = 0.1\%$.

3.2. Volume-preserving strain

Volume-preserving strain is another heterostrain that is relatively common in two-dimensional systems.[24] The specific forms of volume-preserving strain S_{vp} are listed in Section 2. According to Eq. (10), the materials are strained with a magnitude of ϵ along the direction φ and a magnitude of $-\epsilon$ along the vertical direction φ simultaneously.

The effect of strain S_{vp} for a series of strain magnitudes on the electronic structures of TBG at $\varphi = 30°$ and $\varphi = 60°$ is shown in Fig. 3. Under the action of volume-preserving strain, the variation of the flat band with magnitude ϵ is similar to that of the shear strain, as illustrated in the band structures in Figs. 2(a), 2(b) and 3. However, compared with the results for shear strain, the DOS in Fig. 3 demonstrates the unique influence of volume-preserving strain on the TBG system. When the increasing parameter ϵ is taken into account, the characteristic peaks in the DOS are significantly broadened while moving to higher energies. In addition, the prominent peaks in the

DOS evolve from a single peak to a group of peaks consisting of multiple secondary peaks at $\epsilon > 0.2\%$. Moreover, at the same magnitude ϵ, the shape of the two peak groups changes with strain direction φ, which is most obvious when $\epsilon = 0.4\%$.

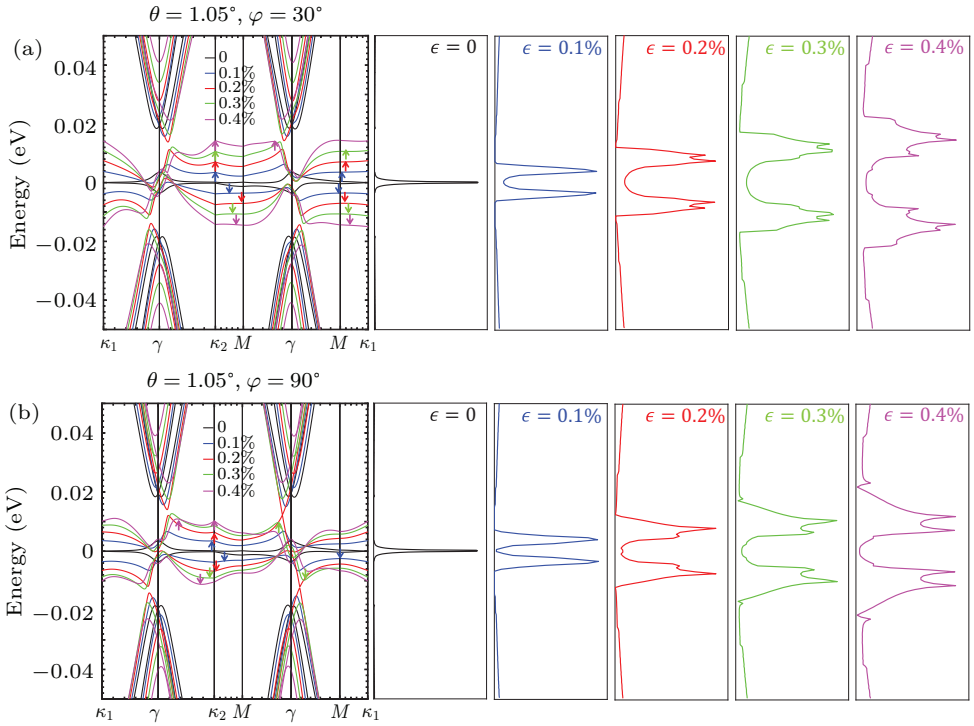


Fig. 3. Band structures and the DOS of magic angle TBG considering volume-preserving strain. (a) Strain direction $\varphi = 60°$ and magnitude $\epsilon = 0$, 0.1%, 0.2%, 0.3%, 0.4%. (b) Strain direction $\varphi = 90°$ and magnitude $\epsilon = 0$, 0.1%, 0.2%, 0.3%, 0.4%. Different colors represent different magnitudes of strain. The colored arrows mark the energy corresponding to the van Hove singularities.

3.3. Biaxial strain

Biaxial strain is a kind of strain in which a low-dimensional system is subjected to stress in both arbitrary and perpendicular directions. In general, biaxial strain is only related to the magnitude ϵ and is independent of the strain direction φ, as derived from Eq. (11).

Figure 4(a) shows the influence of biaxial strain on the electronic structures in TBG under different strain magnitudes ϵ. Unlike shear strain and volume-preserving strain, biaxial strain does not open the band gap of TBG at the k_1 point. As shown in Fig. 4(c), since the threefold rotational symmetry is not broken when biaxial strain is applied to TBG, the two Dirac crossing points connecting the two energy bands are always located at the corners of the Brillouin zone. Biaxial strain can greatly affect the behavior of the lowest conduction band and the valence band, whereas the remote bands are independent of the strain magnitudes ϵ. Besides, with increase in ϵ, the energy gaps between the two flat bands near the CNP and the remote bands decrease gradually and tend to overlap. In Fig. 4(b), we show the electronic band diagram of TBG with an additional small rotation angle $\Delta\theta$ around the magic angle $\theta \approx 1.05°$. It can be observed that the effect of twisted angle $\Delta\theta$ on electron structures is very similar to that of biaxial strain in TBG. This finding can be attributed to the biaxial strain-induced vector potential $\boldsymbol{A} = 0$, resulting in geometrical biaxial strain effects consistent with the twisted angle. Our results are agreement with previous studies on TBG under biaxial strain.[44]

3.4. Uniaxial strain

Uniaxial strain is a kind of strain in which the bilayer system is subjected to relative stress in one direction but not in the vertical direction. In previous studies,[52,53] uniaxial strain was found to exist extensively in TBG samples. The influence of uniaxial strain on the electronic band structure of TBG has been described in detail in previous works,[17,24,38,42,43] and the most important feature caused by uniaxial strain is the energy separation between the conduction band and the valence band near the CNP.

3.5. Discussion

We have described in detail the characteristics of the band structures in the TBG system under the influence of various strains. Next, we discuss the connections and differences between the dissimilar strains. We can clearly observe that the central flat band of TBG is very sensitive to all strains. Each strain near the magic angle broadens the bandwidth of the central flat band, leading the large energy separation of van Hove singularities in the DOS. These behaviors can be directly observed in STM experiments.[6,8] It is found that shear

strain and volume-preserving strain have similar effects on the electronic structure of TBG, because asymmetric heterostrains $\mathcal{E}_1 = -\mathcal{E}_2 = \mathcal{E}/2$ are taken into account in our calculations. The central flat band splitting of TBG is mainly related to the anisotropic normal component $\epsilon_- = \frac{1}{2}(\epsilon_{xx} - \epsilon_{yy})$ and the shear component ϵ_{xy} of the strain tensor, which has been explained in previous work by using the pseudo Landau level picture of TBG.[39]

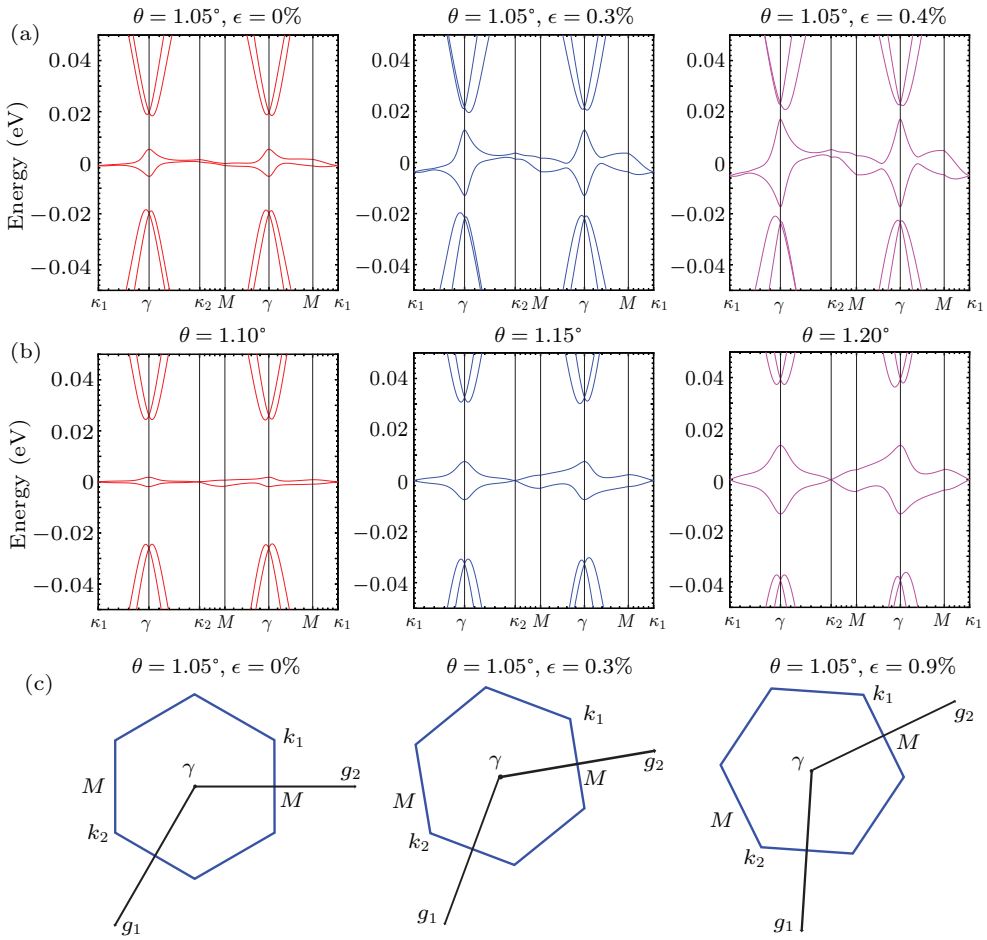


Fig. 4. Band structures of TBG with different (a) biaxial strain magnitudes $\epsilon = 0.1\%, 0.3\%, 0.4\%$ and (b) twisted angles $\theta = 1.10°, 1.15°, 1.20°$. Different colors represent different magnitudes of strain and twisted angle. (c) The moiré Brillouin zone of TBG under various biaxial strain magnitudes ϵ.

We also analyze the differences between the dissimilar strains. Firstly, we find that the bands under different strains have different dispersion. Compared with shear strain, the structure of the van Hove singularity of TBG under volume-preserving strain has broader peaks in the DOS. Secondly, biaxial strain has a very unusual effect on the band of TBG compared with the other three types of strain. Biaxial strain does not break the threefold rotational symmetry of the TBG lattice. The changes in the band and DOS of TBG under the influence of biaxial strain are very similar to the effect of twisted angle. In fact, the geometric effect of biaxial strain is similar to that of twisted angle, as shown in previous studies.[44] Finally, unlike the complete separation of the central flat bands under uniaxial strain, shear strain and volume-preserving strain cause the flat band to change dramatically near the γ point, such that under certain conditions the central flat bands intersect at locations other than the intersection of the two Dirac points. This result means that the electronic and optical behavior of the two flat bands can no longer be considered from the perspective of isolated bands.

4. Conclusion and perspectives

In this paper, we systematically studied the electronic band structure and DOS of magic angle TBG with different types of strain based on the effective continuum model. We find that the flat band near the CNP is greatly sensitive to shear, volume-preserving and uniaxial strain, which leads to distinct behaviors in the flat bands and DOS. Unlike uniaxial strain, the energy transition of shear strain and volume-preserving strain is more intense near the γ point of the central flat band, and the two types of strain have dissimilar strain direction dependences, which enables us to extract a lot of critical information about band structure. In addition, biaxial strain is unusual compared with the other strain modes in that the effect on TBG is very similar to that of the twisted angle both geometrically and electronically, which provides a way to achieve

some twisted angles that are difficult to fabricate experimentally using biaxial strain in the future. Finally, we found that different types of strain lead to corresponding characteristic peaks and thus modify the van Hove singularities in the DOS of the flat bands, which are expected to significantly influence the correlated and topological electronic phases in TBG and can be studied by future STM experiments.[6–8,17]

Acknowledgements

Project supported by the National Natural Science Foundation of China (Grant No. 11874271). We thank Yan He for theoretical support and discussions.

References

[1] Cao Y, Fatemi V, Demir A, Fang S, Tomarken S L, Luo J Y, Sanchez-Yamagishi J D, Watanabe K, Taniguchi T, Kaxiras E, Ashoori R C and Jarillo-Herrero P 2018 *Nature* **556** 80
[2] Cao Y, Fatemi V, Fang S, Watanabe K, Taniguchi T, Kaxiras E and Jarillo-Herrero P 2018 *Nature* **556** 43
[3] Arora H S, Polski R, Zhang Y R, Thomson A, Choi Y, Kim H, Lin Z, Wilson I Z, Xu X D, Chu J H, Watanabe K, Taniguchi T, Alicea J and Nadj-Perge S 2020 *Nature* **583** 379
[4] Cao Y, Chowdhury D, Rodan-Legrain D, Rubies-Bigorda O, Watanabe K, Taniguchi T, Senthil T and Jarillo-Herrero P 2020 *Phys. Rev. Lett.* **124** 076801
[5] Chen G R, Sharpe A L, Fox E J, Zhang Y H, Wang S X, Jiang L L, Lyu B S, Li H Y, Watanabe K, Taniguchi T, Shi Z W, Senthil T, Goldhaber-Gordon D, Zhang Y B and Wang F 2020 *Nature* **579** 56
[6] Choi Y, Kemmer J, Peng Y, Thomson A, Arora H, Polski R, Zhang Y R, Ren H C, Alicea J, Refael G, von Oppen F, Watanabe K, Taniguchi T and Nadj-Perge S 2019 *Nat. Phys.* **15** 1205
[7] Jiang Y H, Lai X Y, Watanabe K, Taniguchi T, Haule K, Mao J H and Andrei E Y 2019 *Nature* **573** 91
[8] Kerelsky A, McGilly L J, Kennes D M, Xian L D, Yankowitz M, Chen S W, Watanabe K, Taniguchi T, Hone J, Dean C, Rubio A and Pasupathy A N 2019 *Nature* **572** 95
[9] Lu X B, Stepanov P, Yang W, Xie M, Aamir M A, Das I, Urgell C, Watanabe K, Taniguchi T, Zhang G Y, Bachtold A, MacDonald A H and Efetov D K 2019 *Nature* **574** 653
[10] Polshyn H, Yankowitz M, Chen S W, Zhang Y X, Watanabe K, Taniguchi T, Dean C R and Young A F 2019 *Nat. Phys.* **15** 1011
[11] Saito Y, Ge J Y, Watanabe K, Taniguchi T and Young A F 2020 *Nat. Phys.* **16** 926
[12] Serlin M, Tschirhart C L, Polshyn H, Zhang Y, Zhu J, Watanabe K, Taniguchi T, Balents L and Young A F 2020 *Science* **367** 900
[13] Sharpe A L, Fox E J, Barnard A W, Finney J, Watanabe K, Taniguchi T, Kastner M A and Goldhaber-Gordon D 2019 *Science* **365** 605
[14] Stepanov P, Das I, Lu X B, Fahimniya A, Watanabe K, Taniguchi T, Koppens F H L, Lischner J, Levitov L and Efetov D K 2020 *Nature* **583** 375
[15] Stepanov P, Xie M, Taniguchi T, Watanabe K, Lu X B, MacDonald A H, Bernevig B A and Efetov D K 2021 *Phys. Rev. Lett.* **127** 197701
[16] Wong D L, Nuckolls K P, Oh M, Lian B, Xie Y L, Jeon S, Watanabe K, Taniguchi T, Bernevig B A and Yazdani A 2020 *Nature* **582** 198
[17] Xie Y L, Lian B, Jack B, Liu X M, Chiu C L, Watanabe K, Taniguchi T, Bernevig B A and Yazdani A 2019 *Nature* **572** 101
[18] Yankowitz M, Chen S W, Polshyn H, Zhang Y X, Watanabe K, Taniguchi T, Graf D, Young A F and Dean C R 2019 *Science* **363** 1059
[19] Zondiner U, Rozen A, Rodan-Legrain D, Cao Y, Queiroz R, Taniguchi T, Watanabe K, Oreg Y, von Oppen F, Stern A, Berg E, Jarillo-Herrero P and Ilani S 2020 *Nature* **582** 203
[20] Bistritzer R and MacDonald A H 2011 *Proc. Natl. Acad. Sci. USA* **108** 12233
[21] de Laissardiere G T, Mayou D and Magaud L 2010 *Nano Lett.* **10** 804
[22] de Laissardiere G T, Mayou D and Magaud L 2012 *Phys. Rev. B* **86** 125413
[23] Morell E S, Correa J D, Vargas P, Pacheco M and Barticevic Z 2010 *Phys. Rev. B* **82** 121407
[24] Bi Z, Yuan N F Q and Fu L 2019 *Phys. Rev. B* **100** 035448
[25] Moon P and Koshino M 2013 *Phys. Rev. B* **87** 205404
[26] Xie M and MacDonald A H 2020 *Phys. Rev. Lett.* **124** 097601
[27] Bultinck N, Khalaf E, Liu S, Chatterjee S, Vishwanath A and Zaletel M P 2020 *Phys. Rev. X* **10** 031034
[28] Carr S, Fang S and Kaxiras E 2020 *Nat. Rev. Mater.* **5** 748
[29] dos Santos J M B L, Peres N M R and Castro Neto A H 2012 *Phys. Rev. B* **86** 155449
[30] Guinea F and Walet N R 2018 *Proc. Natl. Acad. Sci. USA* **115** 13174
[31] Kang J and Vafek O 2018 *Phys. Rev. X* **8** 031088
[32] Koshino M 2015 *New J. Phys.* **17** 015014
[33] Koshino M, Yuan N F Q, Koretsune T, Ochi M, Kuroki K and Fu L 2018 *Phys. Rev. X* **8** 031087
[34] Liu J P and Dai X 2021 *Phys. Rev. B* **103** 035427
[35] Po H C, Zou L J, Vishwanath A and Senthil T 2018 *Phys. Rev. X* **8** 031089
[36] Yu G, Wen L, Luo G and Wang Y 2021 *Phys. Scr.* **96** 125874
[37] Zhang Y, Jiang K, Wang Z Q and Zhang F C 2020 *Phys. Rev. B* **102** 035136
[38] Dai Z B, He Y and Li Z 2021 *Phys. Rev. B* **104** 045403
[39] Nakatsuji N and Koshino M 2022 *Phys. Rev. B* **105** 245408
[40] Huder L, Artaud A, Quang T L, de Laissardiere G T, Jansen A G M, Lapertot G, Chapelier C and Renard V T 2018 *Phys. Rev. Lett.* **120** 156405
[41] Wen L, Li Z and He Y 2021 *Chin. Phys. B* **30** 017303
[42] Kaplan D, Holder T and Yan B H 2022 *Phys. Rev. Res.* **4** 013209
[43] Mannai M and Haddad S 2021 *Phys. Rev. B* **103** L201112
[44] Zhai D and Yao W 2020 *Phys. Rev. Mater.* **4** 094002
[45] dos Santos J M B L, Peres N M R and Castro A H 2007 *Phys. Rev. Lett.* **99** 256802
[46] Nam N N T and Koshino M 2017 *Phys. Rev. B* **96** 075311
[47] Koshino M and Nam N N T 2020 *Phys. Rev. B* **101** 195425
[48] Gao Y, Kim S, Zhou S, Chiu H C, Nelias D, Berger C, de Heer W, Polloni L, Sordan R, Bongiorno A and Riedo E 2015 *Nat. Mater.* **14** 714
[49] Novoselov K S, Mishchenko A, Carvalho A and Neto A H C 2016 *Science* **353** aac9439
[50] Tan P H, Han W P, Zhao W J, Wu Z H, Chang K, Wang H, Wang Y F, Bonini N, Marzari N, Pugno N, Savini G, Lombardo A and Ferrari A C 2012 *Nat. Mater.* **11** 294
[51] Yao J D and Yang G W 2022 *J. Appl. Phys.* **131** 0087503
[52] Frisenda R, Druppel M, Schmidt R, de Vasconcellos S M, de Lara D P, Bratschitsch R, Rohlfing M and Castellanos-Gomez A 2017 *Npj 2d Mater. Appl.* **1** 10
[53] Guinea F 2012 *Solid State Commun.* **152** 1437